remote sensing

MDPI

Technical Note

Revealing the Morphological Evolution of Krakatau Volcano by Integrating SAR and Optical Remote Sensing Images

Jianming Xiang [1], Shaohua Guo [1], Xianlin Shi [1,*], Daijun Yu [1], Guan Wei [1], Ningling Wen [1], Chen Chen [1] and Keren Dai [1,2]

[1] College of Earth Science, Chengdu University of Technology, Chengdu 610059, China; xiangjianming17@cdut.edu.cn (J.X.); guoshaohua@stu.cdut.edu.cn (S.G.); ydj@cdut.edu.cn (D.Y.); guanwei@stu.cdut.edu.cn (G.W.); wenningling@stu.cdut.edu.cn (N.W.); chenchen1@stu.cdut.edu.cn (C.C.); daikeren17@cdut.edu.cn (K.D.)

[2] State Key Laboratory of Geohazard Prevention and Geoenvironment Protection, Chengdu University of Technology, Chengdu 610059, China

* Correspondence: shixianlin06@cdut.edu.cn

Abstract: On 22 December 2018, volcano Anak Krakatau, located in Indonesia, erupted and experienced a major lateral collapse. The triggered tsunami killed at least 437 people by the 13-m-high tide. Traditional optical imagery plays a great role in monitoring volcanic activities, but it is susceptible to cloud and fog interference and has low temporal resolution. Synthetic aperture radar (SAR) imagery can monitor volcanic activities at a high temporal resolution, and it is immune to the influence of clouds. In this paper, we propose an automatic method to accurately extract the volcano boundary from SAR images by combining multi-polarized water enhancement and the Nobuyuki Otsu (OTSU) method. We extract the area change of the volcano in 2018–2019 from Sentinel-1 images and ALOS-2 imagesThe area change and evolution are verified and analyzed by combing the results from SAR and optical data. The results show that the southeastern part of the volcano expanded significantly after the eruption, and the western part experienced collapse and recovery. The volcano morphology change experienced a slow-fast-slow process in the two years.

Keywords: Anak Krakatau volcano; the Nobuyuki Otsu (OTSU) method; multi-polarization; synthetic aperture radar (SAR)

check for updates

Citation: Xiang, J.; Guo, S.; Shi, X.; Yu, D.; Wei, G.; Wen, N.; Chen, C.; Dai, K. Revealing the Morphological Evolution of Krakatau Volcano by Integrating SAR and Optical Remote Sensing Images. *Remote Sens.* **2022**, *14*, 1399. https://doi.org/10.3390/rs14061399

Academic Editors: Chisheng Wang, Daqing Ge, Guohong Zhang, Wu Zhu and Siting Xiong

Received: 9 January 2022
Accepted: 7 March 2022
Published: 14 March 2022

Publisher's Note: MDPI stays neutral with regard to jurisdictional claims in published maps and institutional affiliations.

Copyright: © 2022 by the authors. Licensee MDPI, Basel, Switzerland. This article is an open access article distributed under the terms and conditions of the Creative Commons Attribution (CC BY) license (https://creativecommons.org/licenses/by/4.0/).

1. Introduction

On 22 December 2018, at 21:30 local time, the coastline of the Sunda Strait in Indonesia was stricken by a tsunami, which was brought on by an undersea landslide of Anak Krakatau volcano [1–4]. The tsunami led to 437 casualties, 31,943 injuries and 10 missing people. Over 16,000 people were displaced [5]. Long-term monitoring of volcanic pattern changes may reduce the damage caused by such disasters.

Optical images have high spatial resolution, but they have low temporal resolution and are susceptible to clouds and fog contamination. Synthetic aperture radar (SAR) sensors work with microwave bands that can penetrate clouds and fog, providing better vision than visible light and infrared remote sensing [6,7]. Therefore, SAR images are rapidly developed and widely applied in volcano and landslides monitoring, as well as shorelines and water bodies extraction [8]. The algorithms for extracting water bodies include the sea areas segmentation algorithm based on the Nobuyuki Otsu (OTSU) method and statistical characteristics of sea areas, and the water body extraction algorithm based on thresholds [9–11] or the object-oriented method [12–14]. SAR polarization information is also used to extract the water body [15–19].

The surface deformation caused by volcanic eruptions can be obtained by analyzing the InSAR coherence and backscatter images of Anak Krakatoa [20]. Some ground data and satellite images show that, before the devastating tsunami, flanking motion was evident

along with more frequent volcanic activities [4], which may present as morphology changes. The initial landslide volume led by submarine collapse of the Krakatoa volcano ranged from 0.22 to 0.30 km^3, which was estimated by comparing the satellite and aerial photography images before and after the eruption [1]. Thus, using the multi-polarization information of both optical and SAR images to monitor the volcano morphology change may provide useful information for disaster warning.

In this paper, we use Google images and Planet images before and after the volcanic eruption for visual interpretation and comparative analysis of volcanic morphological changes, and use multi-polarization fused SAR images (Sentinel-1 and ALOS-2) to extract the volcano area change during 2018–2019. We analyze the monthly morphological changes of Krakatoa Island, and the changes before and after the eruption. The results show that after the eruption, the southeastern part of the volcano expanded significantly, and the western part experienced collapse and recovery. The volcano morphology experienced slow-fast-slow changes during the two years.

2. Study Area and Data

2.1. Overview of the Study Area

The Sunda Strait of Indonesia, located between Sumatra and Java, bridges the Java Sea with the Indian Ocean and is a shipping lane from North Pacific countries to East and West Africa or around the Cape of Good Hope to Europe. The Sunda Strait region has accommodated many crustal movements including volcanic activities. Krakatoa volcano at the southern entrance is the most famous one (Figure 1a). Anak Krakatoa is the resurgent volcanic island rising from the caldera formed in the historic 1883 eruption, with flat areas covered in dense vegetation prior to the most recent large eruptions (Figure 1b). On 17 December 2018, the Planet satellite observed the ash eruption from the crater. On 22 December 2018, the volcano started the large eruption sequence that was observed by Sentinel-1A (Figure 1d),with a large amount of ash filling the air (Figure 1c). The southwestern part of the volcano cone collapsed, which later formed a crater lake by the materials floating on the sea surface in the southwestern part of the island, as observed by the Google image acquired on 11 January 2019 (Figure 1e).

2.2. Data

In this study, we use Google images, Planet images, Sentinel-1 images and ALOS-2 images (Figure 2). Two Google images and four Planet images before and after the outbreak are adopted to extract the volcanic boundaries, which are then used to obtain the morphological changes before and after the eruption. Google Earth's satellite imagery is not a single source of data, but an integration of satellite imagery and aerial photography. The effective resolution of the global landscape imagery on Google Earth is usually 30 m, but for large cities, famous scenic areas and built-up areas, high precision imagery is provided with a resolution of around 1 m and 0.5 m.

Planet, the world's largest microsatellite constellation, consists of hundreds of Dove satellites (10 cm $\times$ 10 cm $\times$ 30 cm). Each Dove satellite is equipped with an optical system and camera with the resolution of 3–5 m.

The Sentinel-1 satellite, consisting of two polar orbiting satellites (A and B), was launched by the European Space Agency Copernicus program (GMES). The two sun-synchronous satellites each have revisit cycles of 12 days. The C-band Sentinel-1 satellite can provide continuous images in the Vertical Transmit-Vertical Receive and Vertical Transmit-Horizontal Receive(VV + VH) polarization mode and Interferometric Wide swath (IW) mode during the period of 2018–2019.

We use one ALOS-2 image acquired on 24 December 2018 to capture the morphological change of the volcano after the eruption. The ALOS-2 satellite is the only L-band SAR satellite currently operating in orbit. It has a revisit period of 14 days.

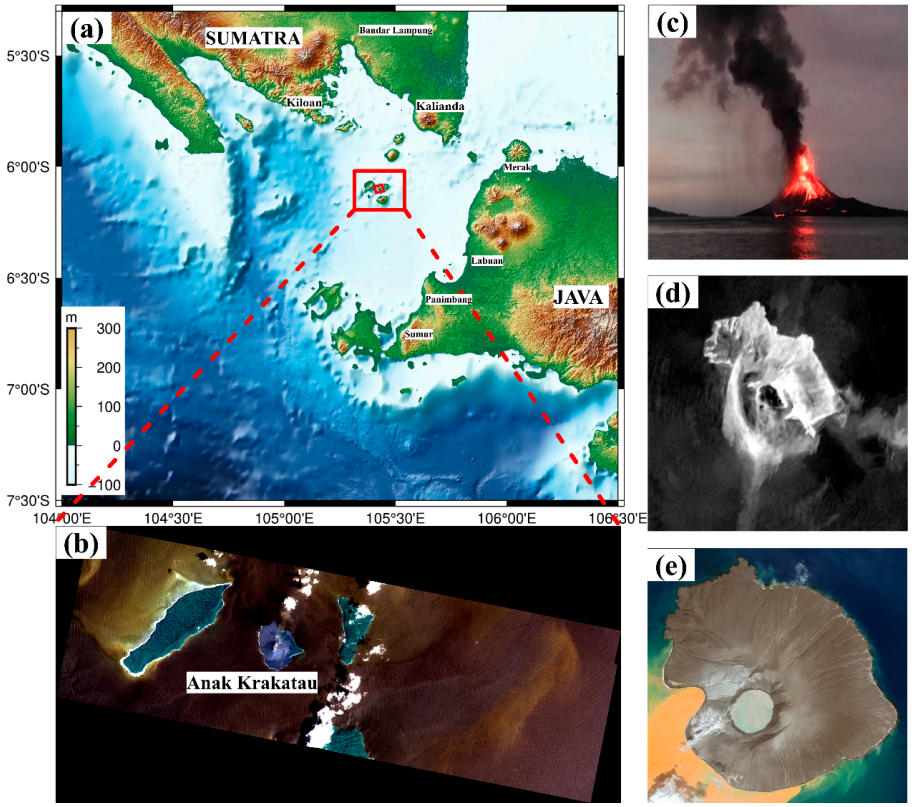

Figure 1. Location map and images of Anak Krakatau volcano. (**a**) Location map; (**b**) volcano before the eruption (Planet image); (**c**) a photo of the volcano eruption (from online source [21]); (**d**) volcano after eruption (synthetic aperture radar (SAR) image); (**e**) volcano after eruption (Google image).

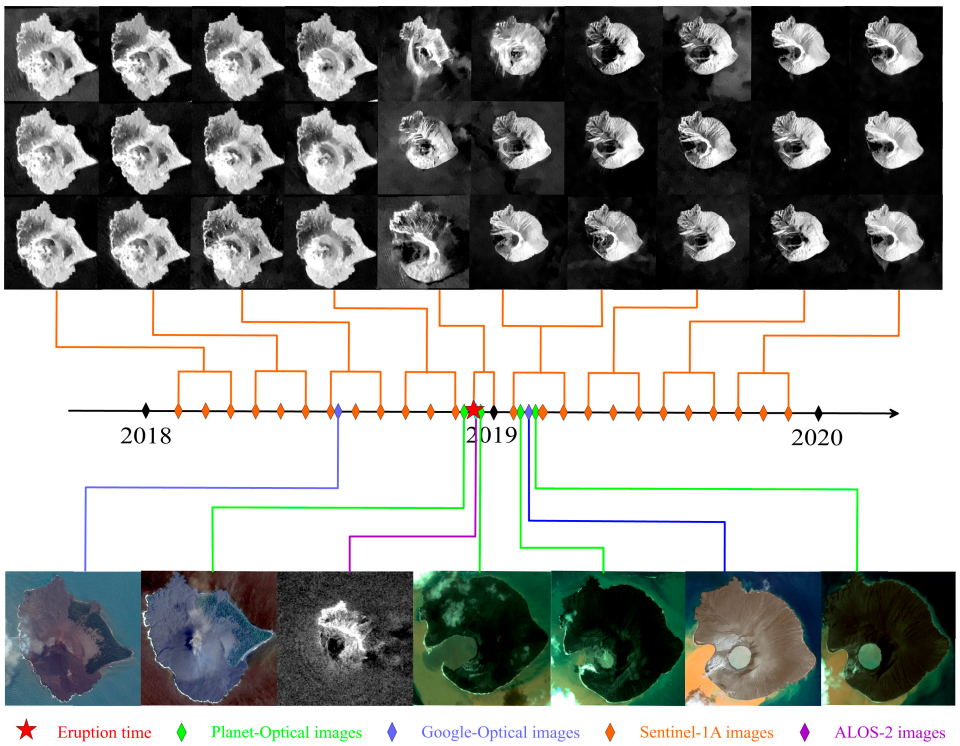

Figure 2. Time chart of the data used in this study, including Planet images, Google images, Sentinel-1A images and ALOS-2 images.

3. Method

We propose a method for volcano morphology extraction on the basis of Sentinel-1 Dual-Polarized Water Index (SDWI) and the Nobuyuki Otsu (OTSU) polarization information enhancement. In this method, the VV and VH polarization of the output SAR image in the IW mode are calculated by band, so as to achieve water body enhancement on the image. The Otsu method is used to search for the best threshold for segmenting the enhanced image. The SAR images can identify water bodies and morphological deformation accurately. Firstly, Sentinel-1A data are preprocessed to obtain the encoded image, which is processed by the SDWI method [15], as shown in Equation (1).

$$k_{sdwi} = \ln(10{*}VV * VH) - 8 \quad (1)$$

Since the backscattering coefficient of water in the SAR image is lower than that of soil and vegetation, the double polarization data is multiplied to enhance the features of water. Then, the Otsu method is used for threshold segmentation using the maximum between class variance of background and target as the criterion. The algorithm is simple, stable and effective [22]. The basic Otsu method is introduced below. Assuming the size of an image is $M * N$, its grayscale range is 0–$L-1$, and the number of the pixels with grayscale i is n_i, then the probability of occurrence of grayscale i is $P_i = n_i/MN$. By setting threshold T to divide the grayscale into target class $C_0 = \{0, 1 \ldots, T-1\}$ and background class $C_1 = \{T-1, \ldots, L-1\}$, we obtain:

The probability of the target part

$$P_0 = \sum_{i=0}^{T-1} P_i \quad (2)$$

The probability of the background part

$$P_1 = \sum_{i=T}^{L-1} P_i = 1 - P_0 \quad (3)$$

The mean value of the target component

$$\mu_0 = \sum_{i=0}^{T-1} iP_i/P_0 \quad (4)$$

The mean value of the background component

$$\mu_1 = \sum_{i=T}^{L-1} iP_i/P_1 \quad (5)$$

The total mean value of image pixels

$$\mu = \sum_{i=0}^{L-1} iP_i + P_0\mu_0 + P_1\mu_1 \quad (6)$$

According to the defining formula of variance as follows:

$$s^2 = \frac{\Sigma(x_i - \overline{x})^2}{n} \quad (7)$$

The interclass variance is

$$\partial^2 = P_0(\mu_0 - \mu)^2 + P_1(\mu_1 - \mu)^2 \quad (8)$$

The formula for the optimal threshold K is

$$K = Arg \max_{0 \le T \le L-1} (\partial^2) \quad (9)$$

Using the maximum interclass variance method in Python, we get the sea–land binary images, with black being the sea surface and white being the volcanic island. On this basis, the classification and post-processing are done in ArcGIS platform to eliminate redundant invalid map spots. The monthly variation of the volcanic area in 2018–2019 is finally calculated. The flowchart of this method is shown in Figure 3.

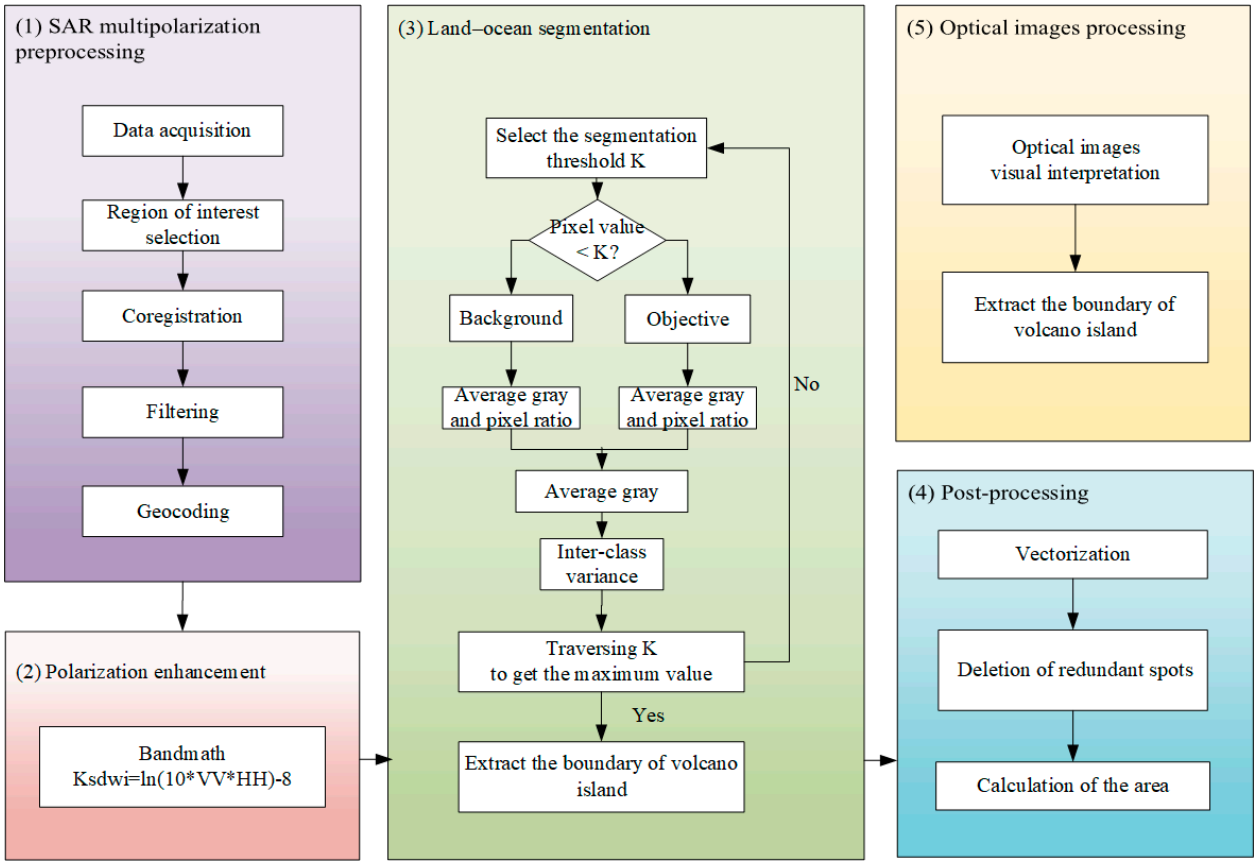

Figure 3. Flowchart of the proposed method.

4. Optical Image and SAR Image Results

4.1. Optical Image Results

After visually interpreting the Planet images (Figure 4a–c) and Google images (Figure 4d–f), we extracted the volcanic morphological changes by vectorization. The eruption smoke is obvious on the Planet image from 17 December 2018 (Figure 4a), indicating that the volcano was in an active period. Similarly, Figure 4c,f shows that the volcano has significant morphological changes after the eruption. The southwestern part of the cone collapsed, the crater formed a concave crater lake and the boundaries clearly expanded eastward and northward.

4.2. SAR Time Series Analysis Results

We calculate the area change of Krakatoa volcano from 2018 to 2019 on the basis of the Sentinel-1A data. The area of the volcano in January 2018 is taken as the initial area (2.86 km^2). The volcanic changes can be divided into the following stages (Figure 5).

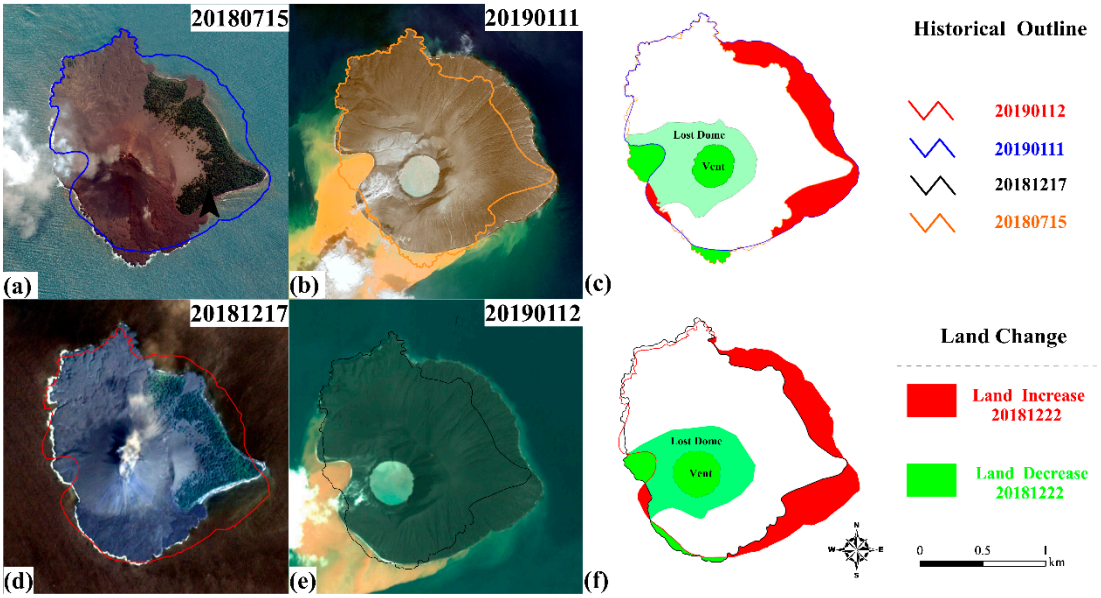

Figure 4. Comparative analysis of optical images: (**a**) the Google image on 15 July 2018; (**b**) the Google image on 11 January 2019; (**c**) morphological changes after eruptions (Google images); (**d**) the Planet image on 17 December 2018; (**e**) the Planet image on 12 January 2019; (**f**) morphological changes after eruptions (Planet images).

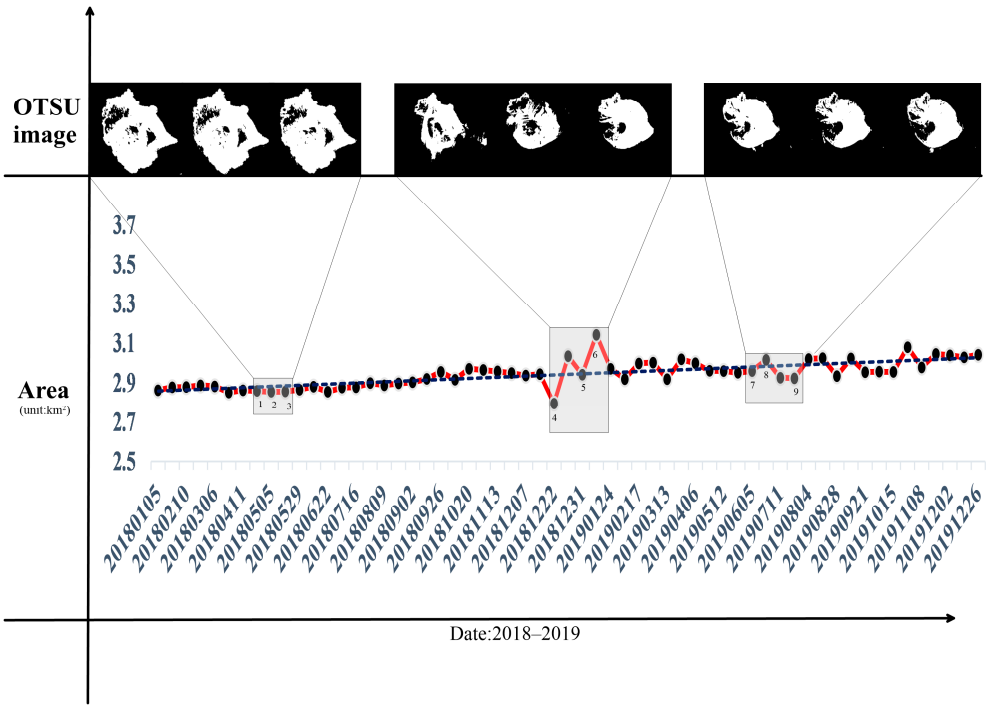

Figure 5. The change of volcanic area from 2018 to 2019 and the comparison of OTSU images and SDWI images at different stages. 1, 2, 3 represent the images of 20180423, 20180505, 20180529, respectively; 4, 5, 6 represent the images of 20181222, 20181227, 20910112; 7, 8, 9 represent the images of 20190629, 20190711, 20190804.

a. Slow volcanic active phase (5 January to 22 December 2018): The area (about 2.85 to 2.97 km^2) grew slowly (before the eruption).

b. Volcano eruption phase (22 December 2018 to 28 December 2018 [23]: On the Sentinel-1A image acquired at 22:34 on 22 December 2018, there are ripples on the sea

surface around the island, and the volcanic plume covering the sky. Accordingly, the volcano was still in a sustained phase of activity until 22:34 p.m. The area of the volcano at that time was minimum due to the collapse of the southwest side and the loss of material. The area was 2.79 km^2, and decreased by 0.15 km^2. According to the analysis in [23], the volcano was active from 16:55 on 22 December to 5:00 on 28 December, which is confirmed by our combined analysis of area, optical images and SAR images.

c. Stable phase after eruption (since January 2019): After the eruption, the eastern and northern parts of the volcano stabilized gradually. The crater formed a closed lake by the material floated back. This crater lake has small changes due to subsequent volcanic activities [24] and ocean currents. During this process, the area of the volcano fluctuated, as shown in the images acquired on NO. 7, 8 and 9 in Figure 5.

The volcano morphological changes occurred in the pre-eruption stage (stage a), the eruption stage (stage b) and the post-eruption stage (stage c). We select the nine images (Figure 5) processed by the SDWI and OTSU methods to show the volcano morphological changes.

4.3. Combined Optical and SAR Image Analysis

For the eruption phase, we combined optical images and SAR images to restore the morphological change process of the volcano (Figure 6).

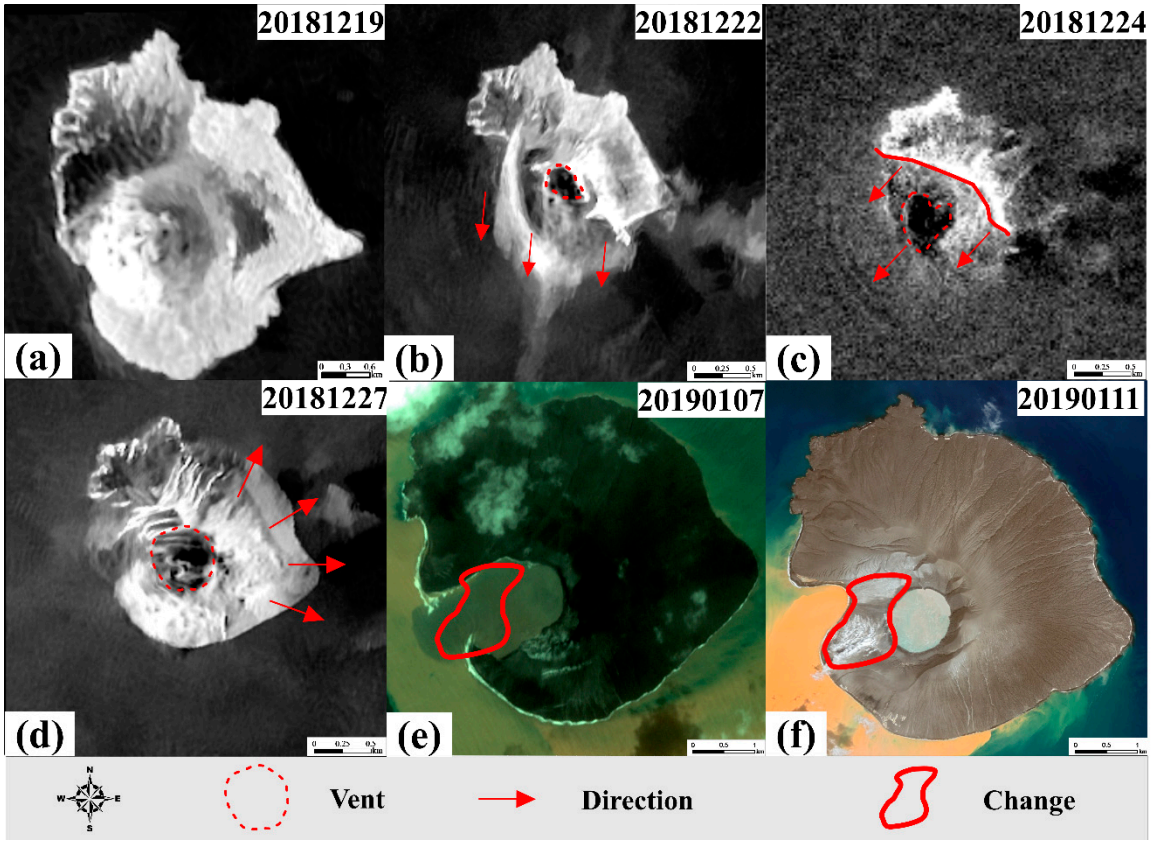

Figure 6. The volcano morphologic changes during the eruption stage analyzed by optical and SAR images. (**a**) the Sentinel-1A image on 19 December 2018; (**b**) the Sentinel-1A image on 22 December 2018; (**c**) the Alos-2 image on 24 December 2018; (**d**) the Sentinel-1A image on 27 December 2018; (**e**) the Planet image on 7 January 2019; (**f**) the Google image on 11 January 2019.

The Sentinel-1A image on 19 December 2018 shows the state of the volcano before the eruption (Figure 6a). The Sentinel-1A image acquired at 22:34 on 22 December 2018 shows that the volcanic cone has collapsed. The lost material moved to the southwest side (Figure 6b). On 24 December 2018, the volcano could be divided into two parts

(highlighted in red line in Figure 6c), with the southwest side showing signs of overall collapse (Figure 6c). There are some ripples on the sea surface, so the volcano was still active. The volcano shape in the descending orbit image on 27 December 2018 is not much different from that in the subsequent time image (Figure 5), which proves that the eastern part of the island has stabilized on 27 December 2018 (Figure 6d). The Planet image on 7 January 2019 shows an open crater lake with a collapsed gap in the southwestern part of the island (Figure 6e). By 11 January 2019 the gap had closed, as observed by both Google images (Figure 6f).

In general, the eruption started at 13:55 on 22 December 2018, and the volcanic material was being lost until 22:34 on 22 December 2018 [4]. The southwestern part of the volcano collapsed and became a crescent-shaped gap. A large amount of collapsed material piled up on the eastern and northern sides and expanded the volcano area (Figure 6b,c). Some material was driven back by the ocean currents and finally filled up the crescent gap by 11 January 2019. Since then, the volcano area became stable.

5. Accuracy Analysis and Discussion

5.1. Accuracy Analysis

In this paper, the volcanic boundaries are automatically identified by band polarization enhancement combined with the Otsu method. To test the boundary accuracy, optical images and SAR images acquired at the same time are selected for comparison. The optical images are analyzed by visual interpretation (Figure 7a,d), and the SAR images are analyzed by visual interpretation (Figure 7b,e) and automatic identification interpretation separately (Figure 7c,f). As Table 1 shows, extraction accuracy before volcanic eruption can reach 99.14%, and after volcanic eruption can reach 96.25%, which confirms the feasibility of automatically extracting volcanic boundaries from SAR images.

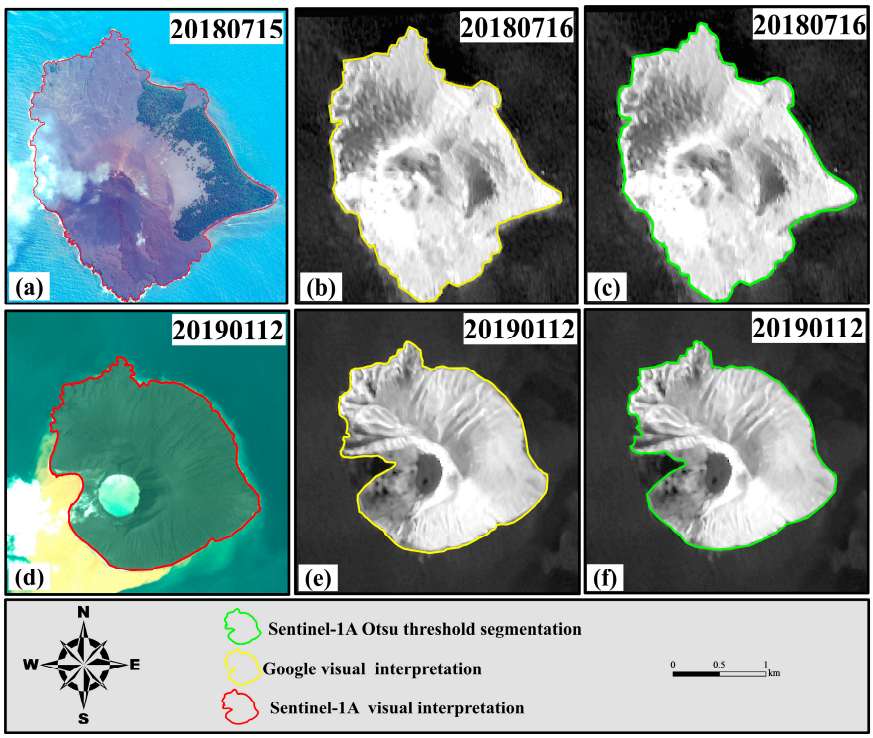

Figure 7. Volcano boundaries extracted from (**a**) the Google image on 15 July 2018 by visual interpretation; (**b**) the Sentinel-1A image on 16 July 2018 by visual interpretation; (**c**) the Sentinel-1A image on 16 July 2018 by the Otus threshold segmentation method; (**d**) the Planet image on 12 January 2019 by visual interpretation; (**e**) the Sentinel-1A image on 12 January 2019 by visual interpretation; (**f**) the Sentinel-1A image on 12 January 2019 by the Otus threshold segmentation method.

Table 1. The volcano area obtained by different methods.

Time	Otus Threshold	Visual Interpretation (km^2)		Difference (km^2)	Relative Accuracy	Average Accuracy
20180716	2.88	SAR image	2.90	0.02	99.31%	99.14%
		Optical image	2.85	0.03	98.96%	
20190112	3.16	SAR image	3.21	0.15	98.44%	96.25%
		Optical image	3.36	0.20	94.05%	

5.2. Discussion

In this paper, four pairs of optical images and SAR images with close acquisition time (maximum interval of one day) are selected to explore the advantages and disadvantages between them, taking Krakatoa Island as an example.

Figure 8a1,a2 shows the images acquired before the eruption. In Figure 8a1, there was vegetation in the eastern part of the volcano, which was covered by a large amount of lava after the eruption. In Figure 8a2, ground objects have sensitive polarization information and high classification accuracy, so the image is suitable for the segmentation of the sea–land boundary. Figure 8b1,b2 shows the post-eruption images, which have the same information. The shadow in the eastern part of the volcanic island in the SAR image is due to the geometric distortion. Both the optical image (Figure 8c1,c2) and SAR image (Figure 8d1,d2) show the formation of the closed crater lake in the southwest. Since SAR images have high temporal resolution and are free of charge, they can be better applied to analyze the morphological changes of long time series. In summary, optical images and SAR images have mutual respective advantages and disadvantages (Table 2), and how to better integrate the advantages of optical images and SAR images for volcano monitoring is worthy of further study.

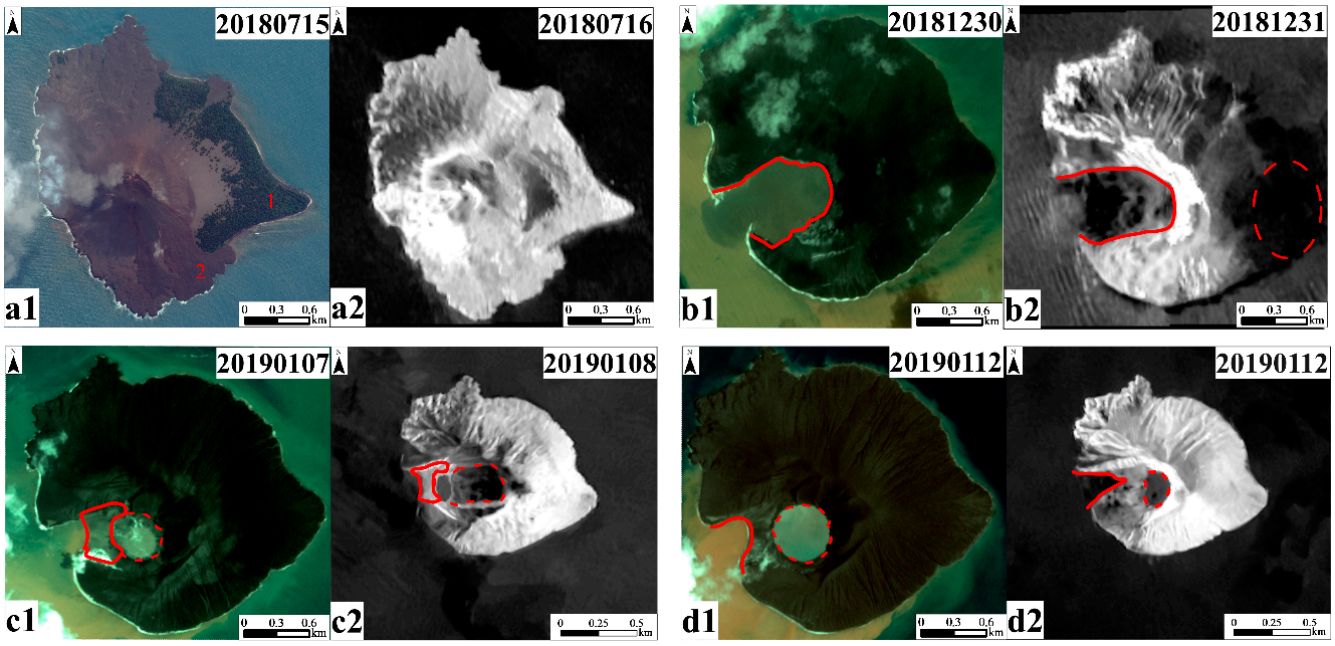

Figure 8. Comparison of optical and SAR images at the same time; optical images for (**a1**,**b1**,**c1**,**d1**); SAR images for (**a2**,**b2**,**c2**,**d2**).

Table 2. Comparison of optical and SAR images.

Data Source	Optical Images	SAR Images
Advantages	1. Rich in texture and spectral information, visually reflecting geomorphological features 2. High spatial resolution, up to 0.3 m	1. All-day, all-weather detection 2. Unaffected by clouds and fog 3. Short revisit period
Disadvantages	1. Effective data constrained by clouds and fog 2. Long revisit period	1. Include geometric distortion areas 2. Geomorphological features are not intuitive
Interpretation method	1. Combine texture, color, shape and other features to interpret 2. Different combinations of bands can be interpreted according to different features	1. Interpretation by amplitude information 2. Fusion interpretation based on polarization information
Applicability	More suitable for areas with lush vegetation and more complex terrain	Suitable for a wide range of flat terrain and perennial cloudy areas

6. Conclusions

In this paper, we use the optical images and SAR images to analyze the morphological changes of Krakatoa volcano before and after the eruption in 2018, by visual interpretation and polarization enhancement combined with the maximum interclass variance method. The polarization enhancement of water body information improves the identification accuracy, and distinguishes water bodies and non-water bodies clearly. The area of Krakatoa was stable before the eruption in December. It grew between 22 December 2018 and 11 January 2019, during which the volcanic morphology also changed greatly. After 11 January 2019, the volcanic morphology became stable. Krakatoa volcano experienced slow to fast and then slow changes in 2018–2019. The volcano eruption had significant impacts on the local climate and people's lives. Timely monitoring of volcanoes is important for volcanic disaster early warning and post-disaster assessment.

Author Contributions: Conceptualization, J.X. and X.S.; methodology, S.G. and D.Y.; software, S.G.; investigation, G.W.; resources, G.W. and K.D.; writing—original draft preparation, S.G. and N.W.; writing—review and editing, K.D., J.X., X.S. and C.C.; funding acquisition, J.X., K.D. and X.S. All authors have read and agreed to the published version of the manuscript.

Funding: This research received no external funding.

Institutional Review Board Statement: Not applicable.

Informed Consent Statement: Not applicable.

Data Availability Statement: Not applicable.

Conflicts of Interest: The authors declare no conflict of interest.

References

1. Grilli, S.T.; Tappin, D.R.; Carey, S.; Watt, S.F.L.; Ward, S.N.; Grilli, A.R.; Engwell, S.L.; Zhang, C.; Kirby, J.T.; Schambach, L.; et al. Modelling of the tsunami from the December 22, 2018 lateral collapse of Anak Krakatau volcano in the Sunda Straits, Indonesia. *Sci. Rep.* **2019**, *9*, 11946. [CrossRef] [PubMed]
2. Robertson, I.; Head, M.; Roueche, D.; Wibowo, H.; Kijewski-Correa, T.; Mosalam, K.; Prevatt, D. *Steer-Sunda Strait Tsunami (Indonesia): Preliminary Virtual Assessment Team (p-Vat) Report*; DesignSafe-CI: Seattle, WA, USA, 2018.
3. Takabatake, T.; Shibayama, T.; Esteban, M.; Achiari, H.; Nurisman, N.; Gelfi, M.; Tarigan, T.A.; Kencana, E.R.; Fauzi, M.A.R.; Panalaran, S.; et al. Field survey and evacuation behaviour during the 2018 Sunda Strait tsunami. *Coast. Eng. J.* **2019**, *61*, 423–443. [CrossRef]

4. Walter, T.R.; Haghshenas Haghighi, M.; Schneider, F.M.; Coppola, D.; Motagh, M.; Saul, J.; Babeyko, A.; Dahm, T.; Troll, V.R.; Tilmann, F.; et al. Complex hazard cascade culminating in the Anak Krakatau sector collapse. *Nat. Commun.* **2019**, *10*, 4339. [CrossRef] [PubMed]
5. Tsunami Sunda Strait (Update 14 January 2019). Available online: https://bnpb.go.id/ (accessed on 6 May 2019).
6. Dai, K.; Li, Z.; Xu, Q.; Bürgmann, R.; Milledge, D.; Tomás, R.; Fan, X.; Zhao, C.; Liu, X.; Peng, J.; et al. Entering the era of Earth observation-based landslide warning systems: A novel and exciting framework. *IEEE Geosci. Remote Sens. Mag.* **2020**, *8*, 136–153. [CrossRef]
7. Deng, H. Application of High Precision Satellite Remote Sensing Technology in Geological Disaster Investigation and Evaluation. Ph.D. Thesis, Chengdu University of Technology, Chengdu, China, 2007.
8. Wu, Y.; Liu, Z. Research progress on methods of automatic coastline extraction based on remote sensing images. *J. Remote Sens.* **2019**, *23*, 582–602.
9. Zhai, Q.; Zhang, D.; Tian, H.; Wu, K.; Wang, X.; Liang, P. Optimal Threshold Segmentation Method for Flood Inundation Range of Multi-exponential Shadow Sentinel-1 SAR Data: Take Shaoyang County as an example. *Mapp. Spat. Geogr. Inf.* **2020**, *43*, 79–83, 86.
10. Chen, L.; Liu, Z.; Zhang, H. SAR image Water Extraction based on Scattering Characteristics. *Remote Sens. Technol. Appl.* **2014**, *29*, 963–969.
11. Jing, B.; Ning, W. Water Body Information Extraction of SAR Images Based on Threshold Segmentation and Decision tree. *Geospat. Inf.* **2021**, *19*, 46–49.
12. Zhu, J.; Guo, H.; Fan, X.; Ding, C.; Ligang, L.; Li, L. Water detection with high-resolution SAR image based on texture and imaging knowledge. *Adv. Water Sci.* **2006**, *04*, 525–530.
13. Wang, J.; Wang, S.; Wang, F.; Zhou, Y.; Ji, J.; Xiong, Y.; Wang, Z.; Zhao, Q. Flood Inundation Region Extraction Method based on Sentinel-1 SAR data. *Disaster Sci.* **2021**, *36*, 7.
14. Wang, H. Water Body Change Detection Based on Ascending and Descending SAR Wavelet Fusion Imagery. Master's Thesis, Nanjing University, Nanjing, China, 2012.
15. Jia, S.; Xue, D.; Li, C.; Zheng, J.; Li, W. Study on new method for water area information extraction based on Sentinel-1 date. *Peoples Yangtze River* **2019**, *50*, 213–217.
16. Zeng, L.; Li, L.; Wan, L. Fast extraction of flood inundation extent based on Sentinel-1 satellite SAR data. *Geogr. World* **2015**, *22*, 100–103, 107.
17. Jiang, J.; Zhou, J.; Yang, B. Automatic Extraction of water Boundary based on Radar Image. *Mar. Inf.* **2020**, *35*, 20–28.
18. Song, H. Research on Extraction of Typical Land Cover Types with PolSAR—A case Research of Water Body Extraction. Master's Thesis, PLA Information Engineering University, Zhengzhou, China, 2012.
19. Deng, Y.; Zhang, H.; Wang, C.; Liu, M. An Object-oriented Water Extraction Method based on Texture andPolarization Decomposition Feature. *Remote Sens. Technol. Appl.* **2016**, *31*, 714–723.
20. Babu, A.; Kumar, S. InSAR coherence and backscatter images based analysis for the Anak Krakatau volcano eruption. *Multidiscip. Digit. Publ. Inst. Proc.* **2019**, *24*, 21.
21. Garcia, G. Volcano Discovery. Available online: https://www.volcanodiscovery.com/krakatoa/2018/dec/eruption-tsunami/updates.html (accessed on 22 December 2018).
22. Chen, X.; Sun, J.; Yin, K.; Yu, J. Sea-Land Segmentation Algorithm for SAR image Based on Otsu Method and Statistical Characteristic of sea Area. *Data Acquis. Process.* **2014**, *29*, 603–608.
23. Perttu, A.; Caudron, C.; Assink, J.D.; Metz, D.; Tailpied, D.; Perttu, B.; Hibert, C.; Nurfiani, D.; Pilger, C.; Muzli, M.; et al. Reconstruction of the 2018 tsunamigenic flank collapse and eruptive activity at Anak Krakatau based on eyewitness reports, seismo-acoustic and satellite observations. *Earth Planet. Sci. Lett.* **2020**, *541*, 116268. [CrossRef]
24. Darmawan, H.; Worosuprojo, S.; Wahyudi, W.; Harijoko, A. Available online: https://www.researchgate.net/publication/349578183_Morphological_Changes_of_Anak_Krakatau_after_the_22_December_2018_Flank_Collapsed (accessed on 24 February 2021).